UNIVERSITY OF CALIFORNIA,
IRVINE

Partial correlation and partial cross-correlation as multivariate measures of EEG connectivity

THESIS

submitted in partial satisfaction of the requirements
for the degree of

MASTER OF SCIENCE

in Biomedical Engineering

by

Xueying Dai

Thesis Committee:
Associate Professor Beth Lopour, Chair
Adjunct Professor Gregory Brewer
Professor Frithjof Kruggel

2021

TABLE OF CONTENTS

LIST OF FIGURES

ACKNOWLEDGEMENTS

I would like to express my sincere gratitude to my committee chair, Professor Beth Lopour, for her persistent help, continuous support, and patience. Her expertise was invaluable in formulating the research questions and methodology and has encouraged me in all the time of my academic research and daily life. Without her guidance, this thesis would not have been possible.

I would also like to extend my deepest appreciation to my committee members, Professor Frithjof Kruggel and Professor Gregory Brewer, for their insightful comments and advice during this busy period.

Many thanks to the Lopouratory, for always being friendly and helpful. I very much appreciate Derek and Kavya for their relentless support in my research and thesis writing.

I also wish to thank my boyfriend and my family, without whom I wouldn't be the person I am today.

ABSTRACT OF THE THESIS

Partial correlation and partial cross-correlation as multivariate measures of EEG connectivity

by

Xueying Dai

Master of Science in Biomedical Engineering

University of California, Irvine, 2021

Associate Professor Beth Lopour, Chair

Electroencephalography (EEG) is an accessible technique that records neuronal oscillatory activity from the scalp. Functional connectivity (FC) analysis through different metrics can be applied to EEG signals to obtain an in-depth understanding of the brain mechanisms. The resulting functional connectivity network (FCN) is of great interest because it has the potential to serve as a biomarker in brain diseases. However, one unsolved issue is that volume conduction (VC) in the EEG system may lead to spurious connectivity and yield inconsistent FCNs across studies. In order to interpret FCNs with confidence, there is a need to develop connectivity metrics that are immune to VC. VC is the spreading of the electric field through the scalp collected by multiple electrodes simultaneously. Multivariate metrics have been reported to be insensitive to VC by means of removing the effect of confounding variables

when it quantifies the relationship between two variables. Here, we propose a new multivariate metrics Partial Cross-Correlation (PCC), aiming to reduce the effect of VC in the FCNs.

We assessed partial correlation (PC) and PCC as multivariate metrics to construct FCNs by applying these metrics to simulated data and human EEG. The simulated data were generated by the Kuramoto model and Rössler model, two models that represent brain dynamics. The human data consisted of routine EEG studies from 240 healthy infants, aged 0-2 years old. The results are compared to FCNs from other well-established bivariate methods, cross-correlation (CC) and adjusted cross-correlation (ACC). Results show that PC, PCC, and ACC excluding values at zero lag (ACC-e) are all valid choices for the EEG system. PC performs the best against volume conduction among all the metrics in both simulated and human EEG. PCC is similarly insensitive to volume conduction, but it is 100-times slower to calculate compared to PC. ACC-e is the only bivariate metric that can work against volume conduction. It is also the most computationally efficient one, yet with the highest false-negative rate. Overall, we recommend using PC or ACC-e as reliable metrics against volume conduction.

Chapter 1 Introduction

1.1 Electroencephalography (EEG) and its Functional Connectivity Network

Electroencephalography (EEG) is a recording technique to measure the oscillations of brain electrical signals by electrodes from the scalp. It provides an insight into the post-synaptic activity of neurons primarily in the cerebral cortex, and it exhibits unique temporal and spatial characteristics that change with sleep stages (Borbely et al., 1981), tasks (Fitzgibbon et al., 2004), and diseases (Briels et al., 2020). Because it is a low-cost and non-invasive method with high temporal resolution compared to functional magnetic resonance imaging (fMRI) and positron emission tomography (PET), EEG is used in a wide range of clinical applications, including anesthesia monitoring (Jameson & Sloan, 2006), epilepsy diagnosis (S. J. M. Smith, 2005) and sleep studies (Vakulin et al., 2016).

EEG signals are also used to gain insight into the mechanisms of brain function. In particular, they are used to study interactions between distinct regions in the brain, which can help and uncover the large-scale functional architecture of the brain. One way to quantify these interactions is by using Functional Connectivity (FC) analysis, which is a statistical measure of the relationship between neural signals collected from discrete brain regions. There are several analytical measures that can be used for FC analysis, including coherence, correlation, dependence, and causality in the time and frequency domains. Functional connectivity networks (FCNs) constructed though FC metrics can be represented mathematically as graphs with nodes (electrodes) and edges (connectivity values between electrodes), and the network properties can be analyzed with graph theory (GT) measures, such as the degree, clustering coefficient, and small-worldness.

FCN is of great interest because it has the potential to provide diagnostic information in brain diseases (Nunez et al., 2015; Sunwoo et al., 2017; Wang et al., 2017) and mental or neural disorders (Imperatori et al., 2019; Kiiski et al., 2020; Zhang et al., 2021). It can also reveal underlying mechanisms in brain functions as a complement to structural connectivity (Babaeeghazvini et al., 2021). For example, Righi et al. (2014) found that the average linear coherence between frontal and temporoparietal regions at 12 months of age was significantly lower in infants who later met the criteria for autism spectrum disorder (ASD) than infants who did not, while three out of five cognitive characteristics failed to identify the difference between the groups at one year of age.

However, one challenge associated with this approach is that FCN studies using different connectivity measures sometimes have no consensus between them. For example, Michelini et al. (2019) reported that connectivity networks constructed through the imaginary part of coherence was significantly higher in the theta, alpha, and beta bands in adolescents and adults with attention deficit hyperactivity disorder (ADHD) compared to the control group. However, another ADHD study using the weighted phase lag index (wPLI) as the connectivity measure reported the opposite result (Kiiski et al., 2020). This implies the need for careful consideration when applying and interpreting functional connectivity.

1.2 Multivariate Methods Against Volume Conduction

One confounding factor that can contribute to inconsistent FCN results using EEG is the spurious connectivity stemming from volume conduction (VC) (Bastos & Schoffelen, 2016). VC is the spreading of the electric field of a neural source in biological tissues that is measured by multiple electrodes simultaneously. Bivariate measurements such as cross-correlation and coherence may yield false interactions between electrodes when volume conduction is present in

the system. Several studies have reported connectivity methods to reduce the effect of volume conduction in simulated and human EEG systems, such as adjusted cross-correlation (ACC) and coherence (Chu et al., 2012), phase lag index (PLI, Ruiz-Gómez et al., 2019) and multivariate metrics (Haufe et al., 2013). Chu et al. (2012) reported that removing values at zero lag in cross-correlation measurements eliminated spurious values caused by volume conduction without excessively affecting the functional networks in a forward model simulation. PLI is another measure that is less sensitive to volume conduction by discarding phase difference between two signals that center around zero mode π (Stam et al., 2007).

Multivariate metrics apply a different tactic to overcome the influence of VC by controlling and removing the effect of shared factors when calculating the relationship between two variables (Haufe et al., 2013; Jalili & Knyazeva, 2011a; Paula et al., 2020; Sakkalis, 2011). For instance, Omidvarnia et al. (2014) reported that partial directed coherence applied on the orthogonal parts of the signals "removed common components akin to volume conduction." Partial correlation (PC), by its definition, should be effective at minimizing the impact of VC. If the signal from two independent sensors, X and Y, are affected by a confounding variable Z, the bivariate correlation between X and Y will be spuriously high. In contrast, when calculating PC between X and Y while controlling the effect of Z, it will correct for the variance between X and Z and Y and Z, and produce a low or close-to-zero PC value (Cohen, 2014). Other direct multivariate metrics like Granger causality (GC) and directed transfer function (DTF) are also considered by some to be effective against volume conduction, although controversy still exists in whether these measurements of connectivity provide an accurate solution to the problem (Brunner et al., 2016). Here, we are specifically interested in partial correlation (PC) as a

promising FCN measurement for EEG because it is easy to compute and apply to both broadband and band-specific signals.

1.3 Motivation

Recent EEG studies have found that FCNs constructed through partial correlation are different from FCNs calculated by bivariate correlation in terms of network properties, such as clustering coefficient, small-worldness, and modularity index (Jalili & Knyazeva, 2011b). Partial correlation can more accurately reveal the direct connections between brain regions, but as a consequence, it is less effective at measuring indirect connections; therefore, it could serve as a complementary measurement to correlation measurement (Jalili & Knyazeva et al., 2011a). In fMRI, research has identified the difference in FCNs using partial and bivariate metrics (Agastinose Ronicko et al., 2020; Ryali et al., 2012; Sun et al., 2004). However, only a single study has compared partial and bivariate correlation in EEG. Hence, there is a need to understand how the metrics work under systems with various degrees of coupling and volume conduction in both simulated and human EEG to interpret future results with more confidence.

In this study, we assess PC and a newly proposed partial cross-correlation (PCC) as multivariate metrics to construct FCNs. We applied these metrics to simulated data and human EEG. The simulation data were generated by the Kuramoto model and Rössler model. A detailed description can be found in Chapter 3. The human data used in this study consisted of routine EEG studies from 240 healthy infants, aged 0-2 years old. For both the simulated and human data, the results for the two multivariate partial correlation metrics were compared to FCNs from three well-established bivariate methods: cross-correlation (CC), adjusted cross-correlation including values at zero lag (ACC-i), and adjusted cross-correlation excluding values at zero lag (ACC-e).

The paper is organized as follows: Chapter 2 first describes the applied functional connectivity metrics, including four existing methods and one novel method, as mentioned in the previous paragraph. Then, detailed information on the simulated data and human data is discussed in Chapters 3 and 4. We then describe the procedure for processing the data and deriving the FCNs in Chapter5. Chapters 6 report results from the simulation model and human data, respectively. Chapter 7 discusses and concludes the paper.

Chapter 2 Connectivity Metrics

2.1 Bivariate Measurements

2.1.1 Cross-Correlation (CC)

Cross-correlation (CC) measures the amplitude-based correlation as a function of time displacement between two time series signals. When the two signals are the same, it is also called autocorrelation. It is a simple way to calculate functional connectivity that has been applied to EEG, fMRI, and Near-infrared spectroscopy (Hyde & Jesmanowicz, 2012; Kumagai et al., 2017; Lu et al., 2010). The cross-correlation value between signals $x(t)$ and $y(t)$ at time lag τ can be expressed as

$$r_{xy}(\tau) = \frac{1}{N-|\tau|}\sum_{t=1}^{N-\tau}(x(t+\tau)-\bar{x})\,(y(t)-\bar{y})\,,$$

where N is the signal length, $\bar{x}$ and $\bar{y}$ are the averages of the signals. The values of $x(t)$ and $y(t)$ are zero-padded when t is out of range. Within a pre-defined range of time lag τ, the maximum of the absolute value is considered the coupling strength between two signals. Our study set the maximum time shift to be either a lead or lag of 200 milliseconds, based on the expected temporal properties of physiological effects (Chu et al., 2012). Given this, the coupling strength between $x(t)$ and $y(t)$ measured by cross-correlation can be calculated by:

$$CC_{xy} = max_{\tau}\left|r_{xy}(\tau)\right|, \tau \in [-200ms, 200ms].$$

2.1.2 Adjusted Cross-Correlations (ACC)

Adjusted cross-correlation is a modified version of CC proposed by (Kramer et al., 2009).The CC_{xy} is adjusted by the Fisher transformation and autocorrelation of the signal, so the values of the coupling strength are closer to a standard normal distribution. ACC can be expressed as:

$$ACC_{xy} = \frac{CC_{xy}^F}{(\widehat{var}(CC_{xy}^F))^{1/2}},$$

where CC_{xy}^F is the Fisher transformation of CC_{xy}

$$CC_{xy}^F = \frac{1}{2} ln \frac{1+CC_{xy}}{1-CC_{xy}},$$

$\widehat{var}(CC_{xy}^F)$ accounts for the effect of autocorrelation on the cross-correlation value

$$\widehat{var}(CC_{xy}^F) = \frac{1}{N-\tau_m} \sum_{\tau=-N}^{N} CC_{xx}^F(\tau) CC_{yy}^F(\tau),$$

and τ_m is the lag time corresponding to the maximal cross-correlation value. Perfectly synchronous activity in two EEG channels can occur due to the volume conduction of an underlying neural source. Hence, maximal cross-correlation at $\tau_m = 0$ is an indicator that the coupling strengths are possibly driven by volume conduction. We tested the effect of including (ACC-i) and excluding (ACC-e) coupling strengths at zero lag in simulated and human data as a means of reducing the impact of volume conduction.

2.2 Multivariate Measurements

2.2.1 Partial Correlation (PC)

Partial correlation (PC) is a multivariate method that can be used to construct functional networks. PC calculates the correlation between two variables while accounting for the effects of other variables, and it can be calculated by taking the inverse of the covariance matrix. Specifically, for a set of variables $\boldsymbol{y} = y_1, y_2, \ldots, y_m$, the precision matrix $\mathbf{P}$ is defined as the inverse of covariance matrix $\mathbf{\Sigma}$:

$$\mathbf{P} = \mathbf{\Sigma}^{-1}.$$

Then the PC between y_i and y_j, which controls for the effects of all other variables that are not y_i and y_j, is defined as the following equation:

$$r(y_i, y_j | \boldsymbol{y}_{-(\boldsymbol{i},\boldsymbol{j})}) = -\frac{p_{ij}}{\sqrt{p_{ii}p_{jj}}},$$

where p_{ij} is the corresponding element in the precision matrix $\boldsymbol{\Sigma}$. In our analysis, we use first-order partial correlation $r(y_i, y_j | y_k)$, which is the correlation value between y_i and y_j controlling for a single variable $y_k (k \neq i, j)$. In an m-node system, each pair of variables has $m - 3$ first-order partial correlation values and one bivariate correlation, i.e., the Pearson correlation $r_p(y_i, y_j)$. The minimal value among these $n - 2$ values is considered the coupling coefficient measured by partial correlation:

$$PC_{ij} = min_k \left| r(y_i, y_j | y_k), r_p(y_i, y_j) \right|, k \neq i, j$$

2.2.2 Partial Cross-Correlation (PCC)

Partial Cross-correlation (PCC) combines the ideas of first-order partial correlation and cross-correlation. The PCC coefficient between y_i and y_j at time lag τ can be expressed as:

$$r\left(y_i(t), \widehat{y_j}(t) \middle| \boldsymbol{y}_{-(\boldsymbol{i},\boldsymbol{j})}(\boldsymbol{t})\right) = -\frac{p_{ij}}{\sqrt{p_{ii}p_{jj}}},$$

where $\widehat{y_j}(t) = y_j(t + \tau), t = 1,2, \ldots N$. When calculating the PCC between any variable pair, $y_j(t)$ is time-shifted by time lag τ before calculating the covariance matrix and partial correlation value. Similar to section 2.1.1, the maximum time shift is either a lead or lag of 200 milliseconds to account for physiological effects. At each time shift, the minimum value among all first-order partial correlations and the bivariate correlation is considered the coupling strength. The procedure was repeated for every time lag. Then the maximum absolute value across time lags was considered the coupling strength PCC_{ij} of the variable pair derived by partial cross-correlation.

Chapter 3 Simulated EEG Data

In this Chapter, we utilized the Kuramoto and Rössler models to generate simulated networks. We created simulated data with the same sampling rate and length as the human data used in this study (Chapter 4). Functional connectivity measurements were applied to the simulated data to verify that they could recover the true connections in the networks. We also introduced various degrees of volume conduction to the simulated data to assess the impact on each measurement.

3.1 The Kuramoto Model

3.1.1 The Kuramoto Model

The Kuramoto model consists of globally coupled oscillators, describing phase relationships similar to neural sources in the human cortex. It has been applied to validate new methods in neuroscience, especially in EEG (Cumin & Unsworth, 2007; Ibáñez-Molina & Iglesias-Parro, 2016; Schmidt et al., 2014). The phase evolution of an M-oscillator system can be described as:

$$\frac{\mathrm{d}\theta_i}{\mathrm{dt}} = \omega_i + \frac{\mathrm{K}}{\mathrm{M}}\sum_{\mathrm{j}=1}^{\mathrm{M}} \sin\left(\theta_j - \theta_i\right) + \delta_i \, , i = 1 \dots M,$$

where θ_i is the phase of oscillator i, ω_i is the intrinsic angular frequency, K denotes the coupling coefficient, and δ_i is the random noise (Kuramoto, 1984). δ_i is selected from a standard normal distribution. For each oscillator, the phase dynamics are defined by its natural frequency as well as the average phase of all other $M - 1$ oscillators. The overall synchrony of the system can be quantified by the phase coherence parameter ϕ:

$$\phi(\mathrm{t}) = \left| \frac{1}{\mathrm{M}} \sum_{\mathrm{j}=1}^{\mathrm{M}} \mathrm{e}^{\mathrm{i}\theta_{\mathrm{i}}(\mathrm{t})} \right|,$$

where $\phi(\mathrm{t})$ can be averaged across time to produce a single value ϕ. The ϕ value is between zero and one, where zero denotes equally distributed oscillator phases around the unit circle, and one consists of perfect phase coupling. The theoretical value of ϕ has a mathematical relationship with K under the assumption that the number of oscillators $M \to \infty$:

$$\phi = \begin{cases} 0, K < K_{crit} \\ \sqrt{1 - \frac{K_{crit}}{K}}, K \geq K_{crit} \end{cases}.$$

The formula to calculate K_{crit} depends on the distribution of natural frequencies. When ω_{i} is picked from a Lorentzian distribution,

$$f(\omega) = \frac{\gamma}{\pi[\gamma^2 + (\omega - \omega_0)^2]},$$

where γ is the half-width at half-maximum in the probability distribution function and the critical coupling strength $K_{crit} = 2\gamma$. When the coupling strength of the system $K < K_{crit}$, the oscillators in the system become unsynchronized, resulting in $\phi = 0$. When $K \geq K_{crit}$, a subset of the oscillators will become synchronized, with the number of oscillators synchronized proportional to K, resulting in a larger ϕ value.

Linear mixing is introduced to the oscillators to model volume conduction under the assumption that all underlying sources are oriented normal to the cortical surface and contribute equally to the electrodes (Ahmadi et al., 2019; Peraza et al., 2012). For an M-oscillator system, the corresponding M-channel EEG signal was generated by incorporating various degrees of linear mixing. The EEG signal $\mathrm{V_i(t)}$ for channel i was calculated using the following equation:

$$V_i(t) = \frac{1}{2i_0 + 1} \sum_{j=i-i_0}^{j=i+i_0} O_j(t)\,,\ i\ =\ 1 \dots M$$

where $2i_0 + 1$ is the number of oscillators contributing to each EEG channel. In neighboring EEG channels, the number of shared oscillators is $2i_0$, resulting in a system with stronger influence due to volume conduction as i_0 increases. $O_j(t)$ is the amplitude of oscillator j and is expressed by the following equation:

$$O_j(t) = Asin\big(\theta_i(t)\big),\ j\ =\ 1 \dots N.$$

Note that for simplicity, we set $A\ =\ 1$ for all oscillators.

3.1.2 Model Simulation

We performed simulations using the Kuramoto model with $N = 19$ oscillators. The intrinsic frequencies of the oscillators were randomly selected from a Lorentzian Distribution with $\omega_0 = 4\pi$, and $\gamma = 2\pi$. This corresponds to an angular frequency of $[2\pi, 6\pi]\ rad/s$, which is an ordinary frequency of 1Hz to 3Hz to approximate the delta band of an EEG signal. The sampling frequency was chosen to be 200 Hz to match the human data. We generated 10-second segments of data, and the first eight seconds of each segment were discarded to remove the initial transients in the system. Only the final two seconds were retained for further analysis. To measure the performance of the different connectivity metrics, we varied the coupling strength K from zero to 30 with a step size of one. We also introduced different levels of linear mixing when generating simulated EEG signals. Specifically, we chose i_0 in the range of zero to three to model different levels of volume conduction.

For each pair of K and i_0 values, five trials were completed. In each trial, we first produced simulated data with 120 two-second epochs. Each epoch was demeaned and divided by the standard deviation before calculating the functional connectivity values as described in chapters

2.1-2.2. To calculate an overall degree of synchronization per pair of K and i_0 values, the functional connectivity matrices were first averaged across trials and then averaged across channel pairs to produce a single value. In this thesis, we use the terms degree of synchronization and mean connectivity interchangeably.

3.2 The Rössler Oscillator

3.2.1 The Rössler Oscillator

The Rössler model has also been used to simulate EEG for the purposes of validating functional connectivity methods. The equations for an M-attractor Rössler model are given by:

$$\begin{cases} \dot{X}_j = -\omega_j Y_j - Z_j + \left[\sum_{i \neq j} \varepsilon_{ij}\left(X_i - Y_j\right)\right] + \sigma\delta_j \\ \dot{Y}_j = -\omega_j X_j - \alpha Y_j \\ \dot{Z}_j = b + \left(X_j - c\right)Z_j \end{cases} , j = 1 \ldots M.$$

When parameters α, b and c are properly chosen, the attractors in the system will oscillate. Eight 6-node networks were used to mimic various connectivity levels and structures based on (Al-Khassaweneh et al., 2016; Shahsavari Baboukani et al., 2019), as shown in Figure 1. Network 1 to 8 have increasing connectivity levels. Network 1 in Fig 1(a) has the lowest synchronization, while network 8 in Figure 1(h) has the highest one. Networks 3, 4, and 5 should have similar degrees of synchrony, but network 3 has a single common source (node 1) for all connections, which may lead to the presence of spurious indirect connections in bivariate connectivity networks.

3.2.2 Model simulation

In the simulation, we set $a = 0.35, b = 0.2, c = 10, \sigma = 1.5, \delta_j$ were randomly selected from the standard normal distribution, and the Rössler attractors will exhibit chaotic dynamics. The connections between oscillators can be modified by ε_{ij}, where $\varepsilon_{ij} = 0.5$ when oscillator i and

j are coupled, and $\varepsilon_{ij} = 0$ otherwise.

We ran 100 iterations of the model simulation for each of the eight network configurations. The sampling frequency was set to 200 Hz to be consistent with the human data. Similar to the Kuramoto model, we created simulated data with 120 two-second epochs in each iteration. Each two-second epoch was demeaned and divided by its standard deviation before analysis.

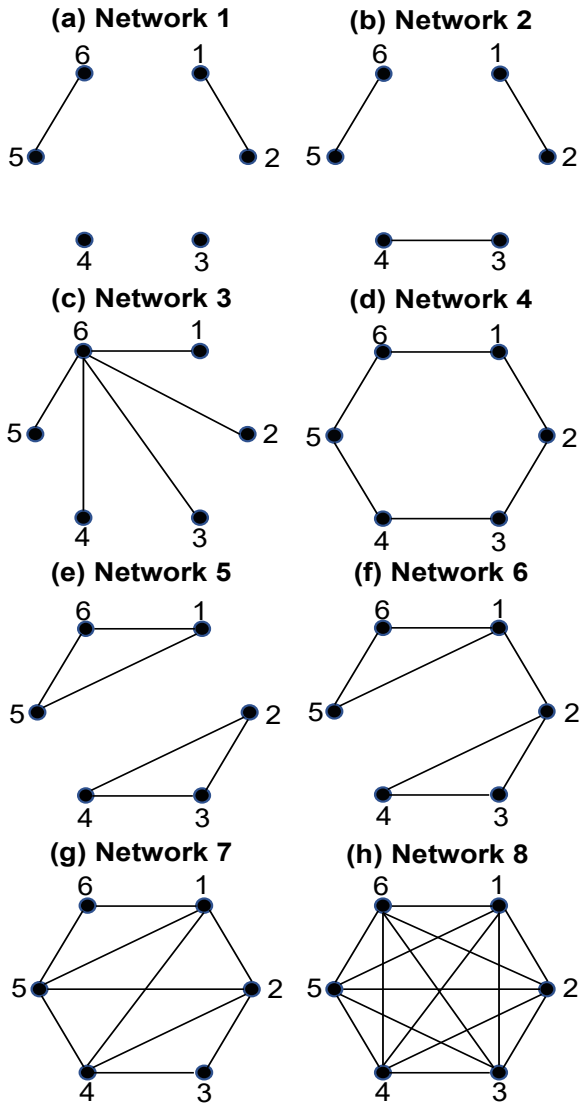

Figure 1 Network Configuration of the Rössler Model derived from Al-Khassaweneh et al. (2016) and Shahsavari Baboukani et al. (2019). The degree of synchronization increases from Network 1 to 8.

Chapter 4 Human EEG Data

4.1 Subject Information

EEG data were collected at the Children's Hospital of Orange County (CHOC), and the Institutional Review Board at CHOC approved its use for this study. Retrospective data from 240 subjects aged 0-24 months were included in the dataset. All subjects were full term (gestational age>38 weeks) with no known neurological disorders. The infants were evenly separated into eight age groups of 30 infants in three-month intervals, i.e., Group A is subjects from 0-3 months old, Group B is 3-6 months old, Group C is 6-9 months old, Group D is 9-12 months old, Group E is 12-15 months old, Group F is 15-18 months old, Group G is 18-21 months old, and Group H is 21-24 months old.

EEG recordings consisted of routine clinical recordings lasting one to two hours, containing a mix of wakefulness and sleep. All EEG recordings were interpreted as normal by a board-certified pediatric epileptologist. Manual EEG sleep staging was performed by a registered polysomnographic technologist using the American Academy of Sleep Medicine (AASM) guidelines. For the subjects in Group A, who were all less than three months old, EEG segments were categorized as wakefulness (W), active sleep (AS), and quiet sleep (QS). For subjects in Group B to H, EEG segments were categorized as wakefulness (W), stage 1 (N1), stage 2 (N2), stage 3 (N3), and rapid eye movement (REM).

4.2 EEG Acquisition and Preprocessing

EEG recordings (Nihon Kohden EEG acquisition system) were acquired at a sampling frequency of 200 Hz, with the exception of a single recording which was acquired at 500 Hz and downsampled to 200 Hz prior to analysis. Nineteen electrodes were placed according to the international 10-20 system in locations Fp1, Fp2, F3, F4, C3, C4, P3, P4, O1, O2, F7, F8, T3, T4,

T5, T6, Fz, Cz, and Pz. Data were bandpass filtered from 0.5-55 Hz and re-referenced to the common average before analysis. Artifacts were identified by applying an automatic extreme value detection algorithm, which was the same as prior studies (Durka et al., 2003; Moretti et al., 2003; R. J. Smith et al., 2021). Data were then divided into two-second non-overlapping time windows for each subject, and windows containing artifacts or mixed state (e.g., contained both N2 and wakefulness) were excluded. 120 two-second epochs were randomly selected for each subject in each brain state (wakefulness, N2 sleep), separately. Whenever subjects had fewer than 120 epochs of a particular brain state, they were excluded from analysis for that state. Due to the limited number of subjects, sleep stages N1, N3 and REM were excluded from the connectivity analysis.

Chapter 5 Functional Connectivity Networks

5.1 Significance Testing

Significance testing is an important step to exclude spurious connections when calculating FCNs. Before significance testing, the connection strengths between channels were calculated using the methods described in chapters 2.1-2.2. The results were stored in $M \times M \times e$ connection strength matrices for an M-node system with e epochs. Time-shuffled data were used to obtain a threshold of significance for each connection pair. The threshold value was the 95th percentile of the surrogate data distribution generated using either 1000 iterations of time-shuffled epochs for bivariate measurements, or 400 iterations for multivariate measurements. The threshold values were stored in $M \times M$ matrices. An adjacency matrix represents the significant connections in a dataset by binarizing the connection strength matrix, where a connection was considered significant, and the corresponding element was set to one if the connection strength was greater than the threshold, zero otherwise. For adjusted cross-correlation, we also considered an additional approach where the connection was only considered significant and set to one when the connection strength was above the threshold, and it had a lag time $\tau_m \neq 0$. The binarized adjacency matrix was averaged across the third dimension (the epochs) to obtain the functional connectivity matrix, representing the percentage of epochs in which significant connections occurred. There was one functional connectivity matrix for each subject, brain state, and connectivity method (cross-correlation, adjusted cross-correlation including or excluding values at zero lag, partial correlation, and partial cross-correlation).

5.2 Functional Connectivity Head Map for Human EEG

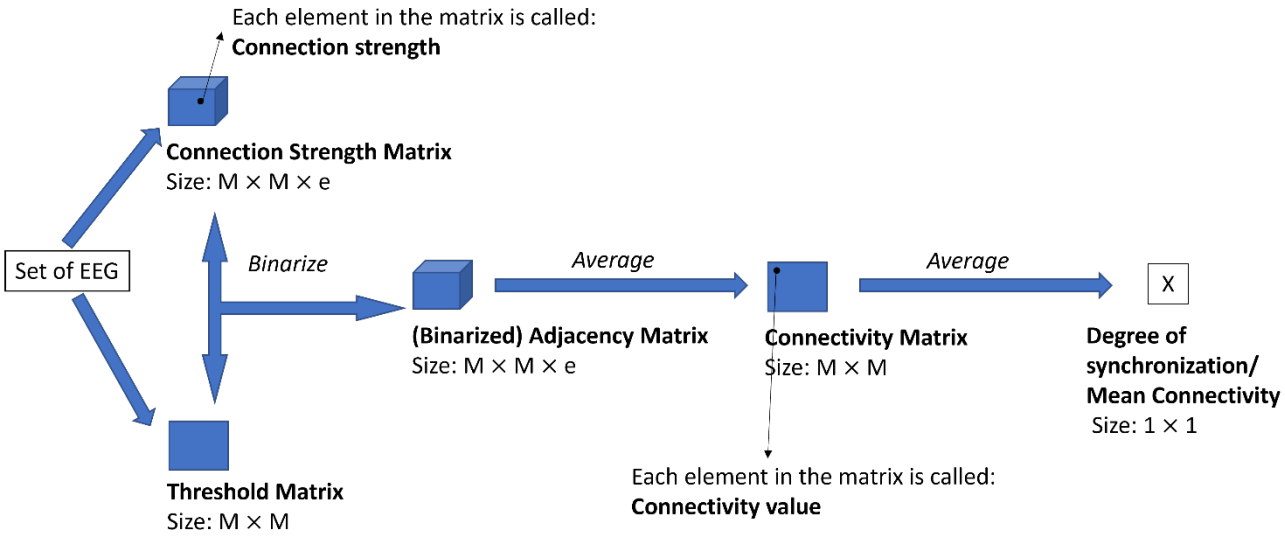

Figure 2 Summary of the functional connectivity analysis, and the related terms.

To visualize the connectivity results for each method, the connectivity matrices were first averaged across subjects in the same age group to produce one matrix per age group and brain state. Then a threshold was applied to these values to convert the averaged connectivity matrices into sparse matrices. This threshold was the top 15% of connectivity values across all age groups in a brain state. Thus, the number of connections for each group may vary based on the overall strength of the average network relative to the other age groups. Finally, the functional connectivity networks were plotted based on the sparse matrices for each connectivity method, age group, and brain state.

Chapter 6 Results

6.1 The Kuramoto Model

The Kuramoto model is a well-established method to simulate brain dynamics. (Nguyen et al., 2020) reported to successfully model and predict features in EEG by the Kuramoto model. Although the Kuramoto model is phase-based, amplitude-based connectivity metrics, such as cross-correlation (Ahmadi et al., 2019), amplitude envelope correlation (Ruiz-Gómez, Gómez, et al., 2019) and S-estimator (Shahsavari Baboukani et al., 2019), have previously been successfully applied to Kuramoto systems. Furthermore, this model includes a method to easily incorporate volume conduction. Hence, we select the Kuramoto model to generate simulated data and see how volume conduction will impact each measurement.

6.1.1 Comparison between connectivity methods

For the simulated EEG based on the Kuramoto model, Figure 3 shows the average degree of synchronization measured by different connectivity metrics as a function of coupling strength K and degree of volume conduction i_0. The phase coherence ϕ is considered the true level of synchronization, and it ranges from 0.2 to 0.8 as K increases (Figure 3A). Based on our settings, the critical value of the system $K_{crit} = 2\gamma = 4\pi$. Theoretically, a system with infinite oscillators will remain uncoupled when $K < K_{crit}$, increase sharply at $K = K_{crit}$, and continuously increase while $K > K_{crit}$. Due to the limited number of oscillators used in our study, we observe a smoother transition in the phase coherence value, which was also reported in (Shahsavari Baboukani et al., 2019).

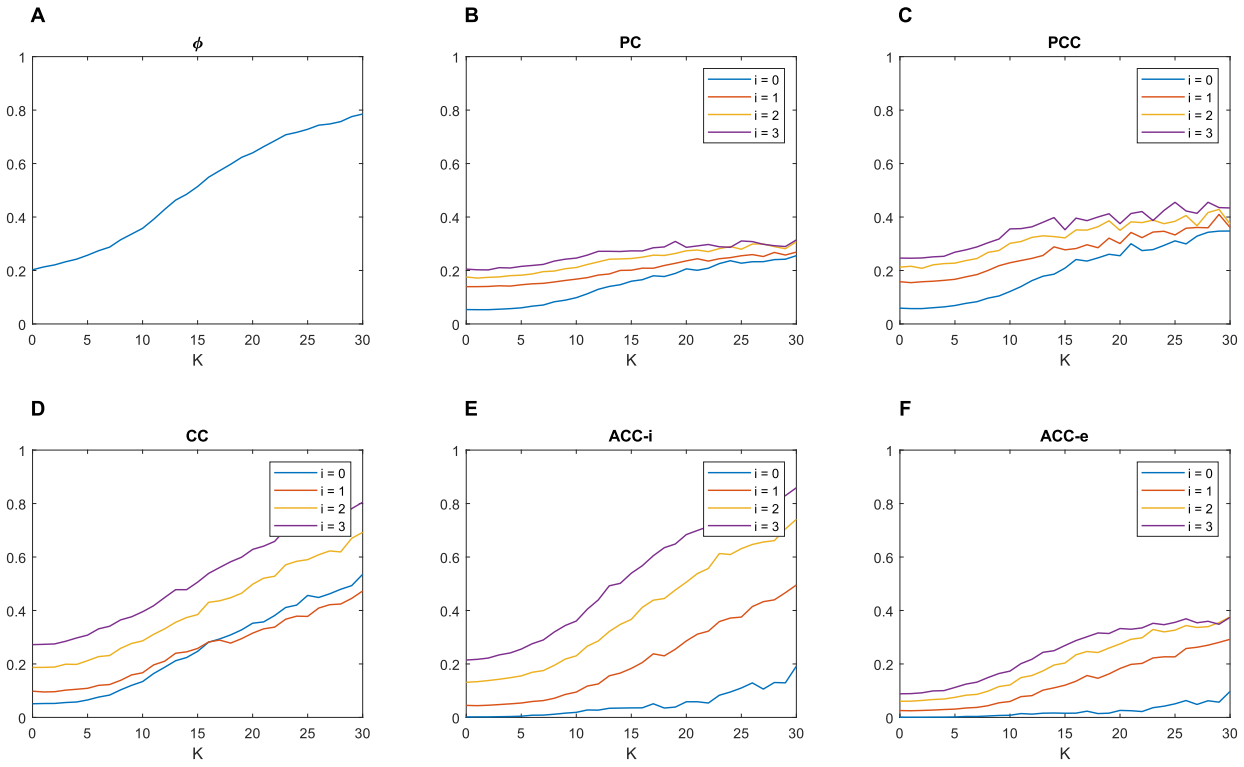

Figure 3 The mean connectivity value of the Kuramoto Model measured by (A) phase coherence, (B) partial correlation, (c) partial cross-correlation, (d) cross-correlation, (e) adjusted cross-correlation including values at zero lag, and (f) adjusted cross-correlation excluding values at zero lag.

The partial correlation metric systematically underestimates the connection strengths, as the curve at $i_0 = 0$ starts around 0.05 and is maximum at 0.26 when (Figure 3B). When i_0 increases, the offset between curves is the lowest in partial correlation compared to all other metrics. For $K < K_{crit}$, the biggest difference occurs when increasing from $i_0 = 0$ to $i_0 = 1$. The degree of synchronization exhibits a smaller difference between i_0 values when $K > K_{crit}$. When $K > 2K_{crit}$, the curves for $i_0 = 2$ and $i_0 = 3$ almost overlap with each other. Thus, the partial correlation appears to be minimally impacted by volume conduction, especially for $K > K_{crit}$. Note that the transition around K_{crit} is not evident in $i_0 > 0$, which indicates that partial correlation is insensitive to volume conduction at the expense of sensitivity to systemic changes.

The partial cross-correlation method performs similarly to partial correlation in that it is not very sensitive to volume conduction. The degree of synchronization associated with this metric is higher than partial correlation and lower than adjusted cross-correlation (Figure 3C).

The results of cross-correlation (Figure 3D) and adjusted cross-correlation including values at zero lag (Figure 3E) are comparable when $i_0 > 0$. The degree of synchronization measured by these two metrics is the closest match to the value of ϕ. However, significant increases in mean connectivity occur as i_0 increases, showing that there is a trade-off between measuring the true level of synchrony and the sensitivity to volume conduction. The performances of the original (Figure 3D) and adjusted cross-correlation (Figure 3E) are notably different for $i_0 = 0$. A possible reason is that when taking the maximum correlation value across time lags, the distribution of the connection strength values deviates farther from a normal distribution (Kramer et al., 2009), and the significance testing is less able to distinguish between coupled and uncoupled connections, especially when the linear mixing in the system is low. Contrary to the original cross-correlation, adjusted cross-correlation accounts for the fact that the maximum values are skewed and corrects the value by the autocorrelation to generate results that are more normally distributed. This primarily affects the results for $i_0 = 0$, and thus, there is a considerable difference between the results for $i_0 = 0$ and $i_0 = 1$.

The impact of excluding connectivity values that are maximal at zero time lag can be inferred by comparing Figures 3E and 3F. It is expected that by excluding a subset of statistically significant connectivity values from the adjacency matrix, the estimated degree of synchronization will be decreased for all K and i_0 values. Consistent with this, we find lower mean connectivity for ACC-e (Figure 3F) compared to the same analysis with those connections included (Figure 3E). The difference is especially significant for large K and i_0 values. The effects of volume conduction

on partial correlation and ACC-e are comparable, although the former is a multivariate measure and the latter a bivariate measure. This suggests that multivariate methods are not required to counteract volume conduction in the system. Also, ACC-e works better for widespread volume conduction ($i_0 = 3$) compared to partial correlation because ACC-e reveals the transition in the system at different K levels, whereas the degree of synchronization revealed by partial correlation has a small, almost constant slope. It is the opposite case when $i_0 = 0$. The results reported here illustrate the importance of understanding the system properties for choosing the most appropriate metric for functional connectivity, as the coupling strength and degree of volume conduction significantly affect the results.

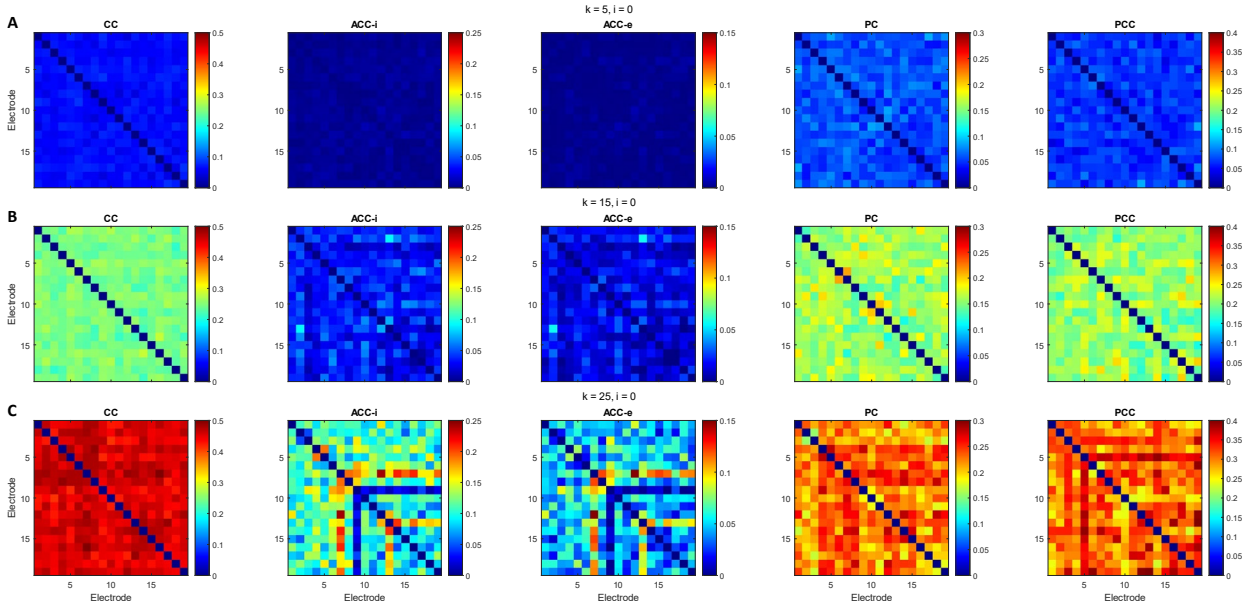

Figure 4 Connectivity Matrices of Kuramoto model data with i set to 0, and (A) K=5, (B) K = 15, (C) K = 25

To understand the connectivity patterns underlying these results, connectivity matrices averaged across five data sets at different K and i_0 values are shown in Figures 4 and 5, where x and y axis corresponds to the electrode index. In Figure 4, i_0 is set to 0, and K equals 5, 15, and

25, respectively, for each row. All metrics successfully demonstrate the expected increase in connectivity strength as K increases, which causes more oscillators to be coupled. Among them, ACC-i and ACC-e have the lowest connectivity values, which aligns with the results in Figure 3.

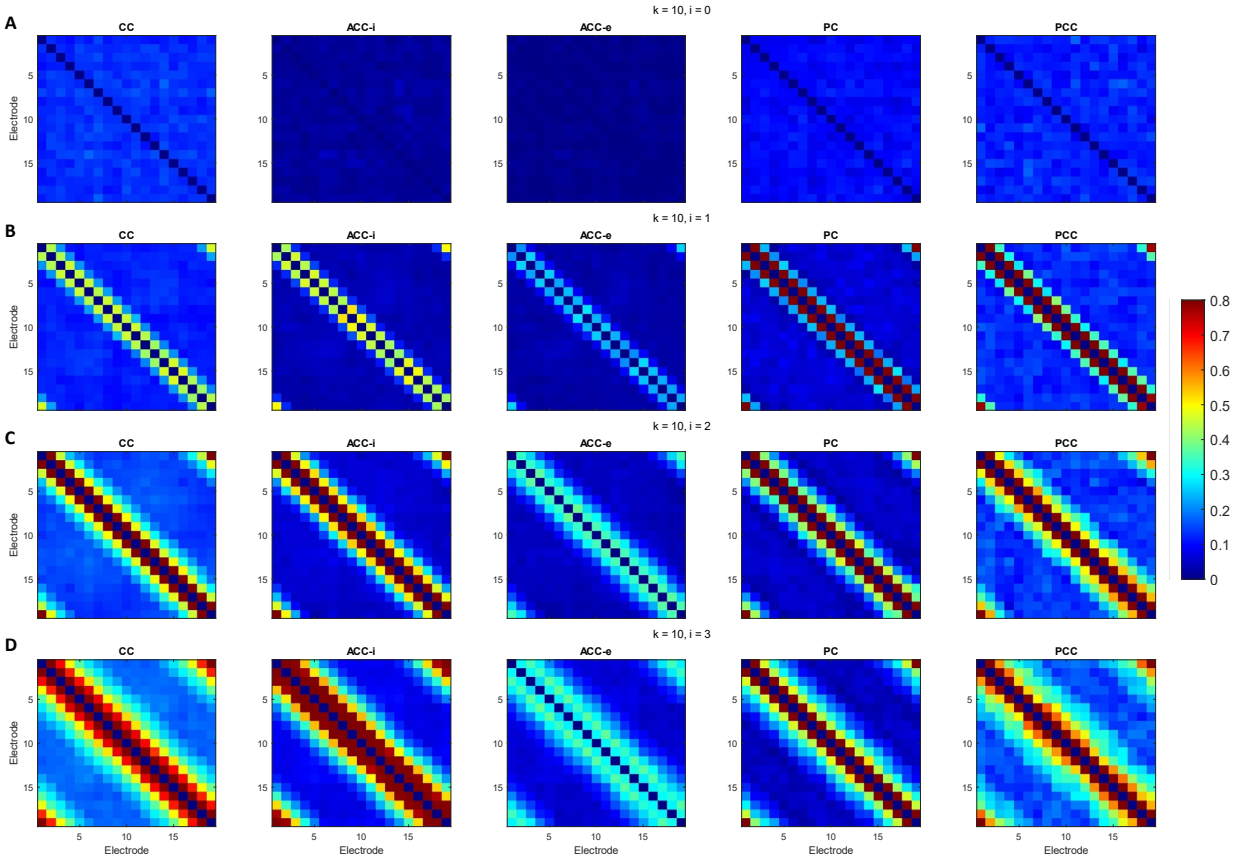

Figure 5 Connectivity Matrices of Kuramoto model data with K set to 10, and (A) i=0, (B) i = 1, (C) i = 2, and (D) i = 3.

In order to compare the effect of linear mixing on each connectivity method, we also show the results for i_0 equals 0, 1, 2, and 3, with K fixed at 10 (Figure 5). Recall that the number of oscillators linearly contributing to the simulated EEG signal equals $2i_0$ Thus, an increase in i_0 simulates a spatially increasing component of volume conduction. The width of the diagonal red-yellow stripe (or blue stripe for ACC-e) represents the spatial spread of increased connectivity due to volume conduction, and it increases as i_0 increases for all measurements. CC, ACC-i, and ACC-

e (Figure 5 A-C) have the same diagonal width, although ACC-e has overall lower connectivity values. Moreover, note that the removal of connections at zero lag in ACC-e is a quite stringent criterion, especially when $i_0 = 3$. It omits some true connections, which causes the lighter blue stripe near the main diagonal. PC has the least amount of spread of all the methods and the highest contrast between the diagonal and background (Figure 5D). The diagonal width of PCC is similar to those of CC and ACC when $i_0 \neq 3$, and is comparable to PC when $i_0 = 3$, although the connection pairs off the main diagonal have higher values compared to PC. This result shows that PCC combines aspects of both PC and CC.

6.2 The Rössler Model

The Rössler model is a non-linear chaotic system that represents a basic coupling mechanism of neurological signals (Lainscsek et al., 2013). This low-dimensional and tunable system can provide insight into how each connectivity method handles direct and indirect connections.

6.2.1 Comparison between connectivity methods

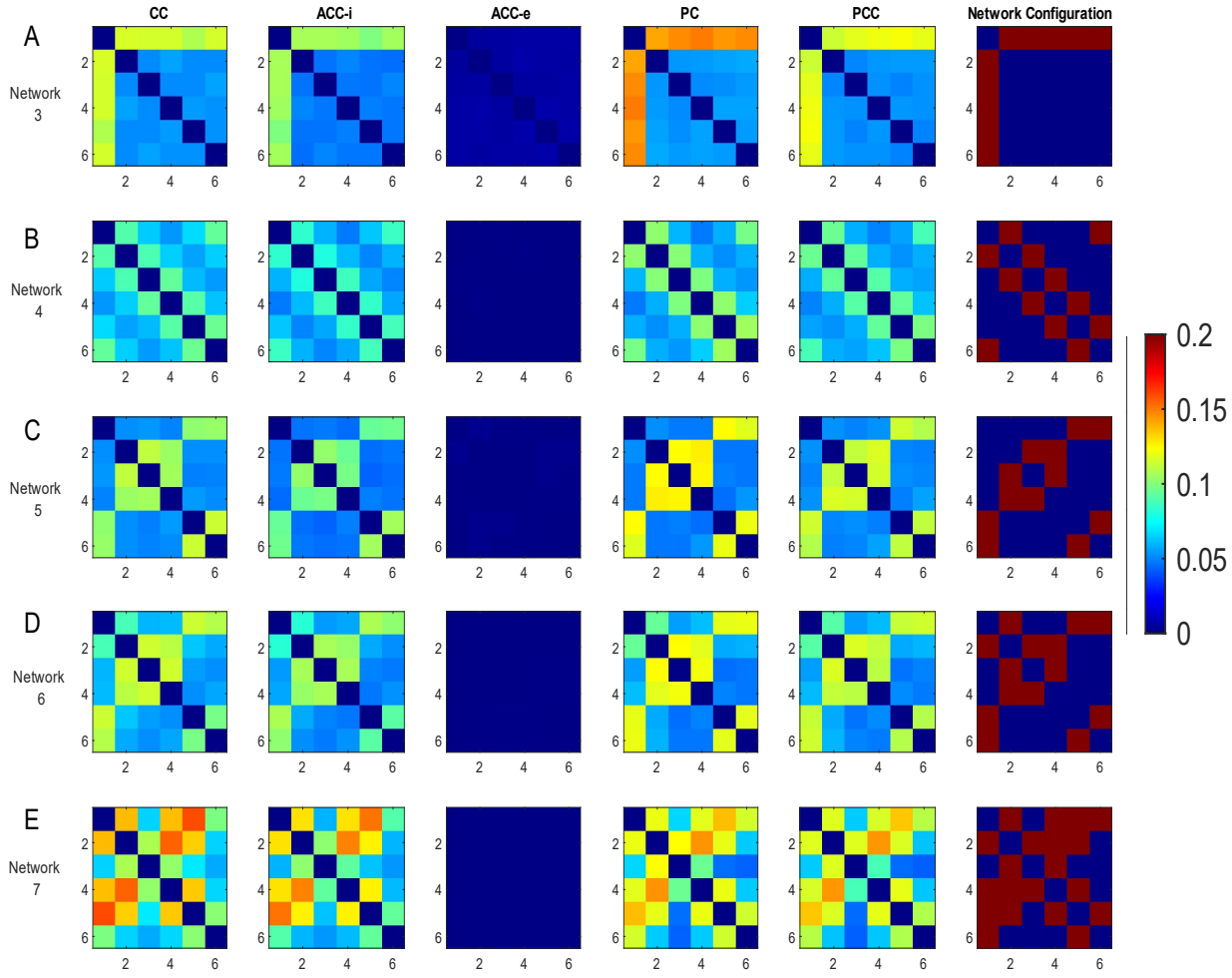

Figure 6 Connectivity Matrices of the Rössler model for network 3-8 (A-E). The most right column shows the actual connections.

Connectivity matrices were averaged across 100 iterations for each method and network configuration (Figure 6). All metrics except ACC-e recover the true connections in the networks. This result may seem to suggest that ACC-e is an invalid metric in the Rössler model, but the reason the connectivity values are so low is that the simulated systems are truly coupled at zero lag. In networks 4-8, over 98% of the statistically significant connections happen at zero lag (see Appendix A). Hence, excluding values at zero lag will remove most of the connections.

However, in real EEG signals, the true connections frequently occur at non-zero lags, so ACC-e will still be a valid measure for that data. Again, it shows the importance of understanding the system under examination in order to choose the best metric.

In general, from network 1 to network 8, the connectivity values increase as the number of connections increases, as expected. One exception to this is that the connectivity values of direct connections in network 3 are higher than those in network 4 for all metrics. This is expected because network 3 has one shared confounding variable for all nodes (Node 1), while the confounding variable in network 4 is different for each pair of nodes. However, note that none of the connectivity methods produce spurious connections between nodes that are driven by a common source. For example, in Network 3, because Node 1 is connected to both Nodes 2 and 3, we might expect that the bivariate connectivity methods would report a connection between Nodes 2 and 3, but this does not occur for any of the methods.

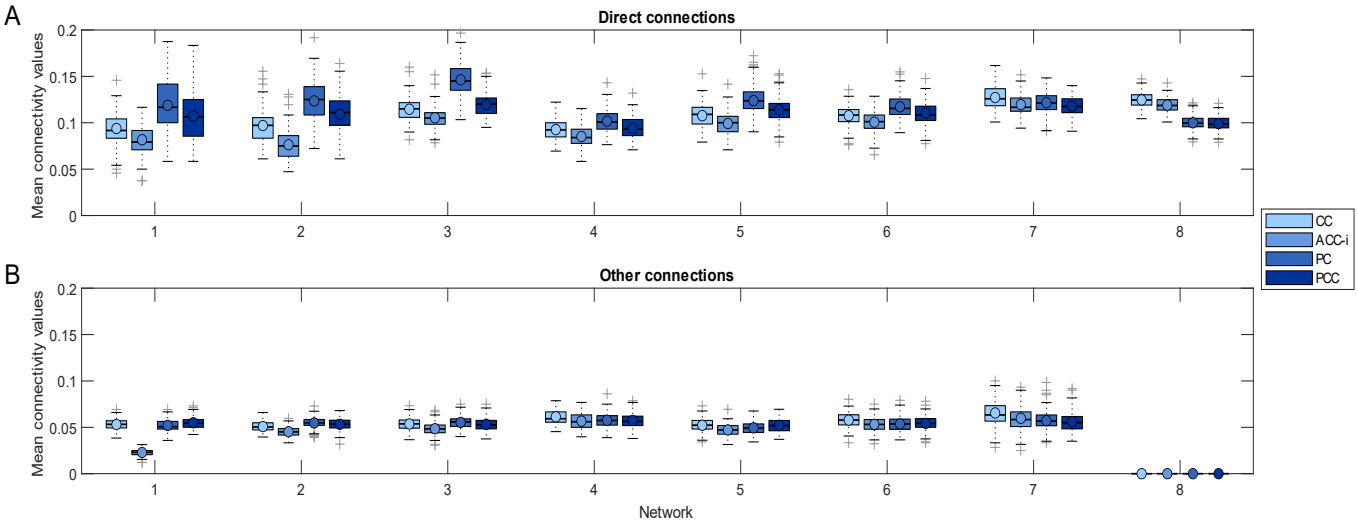

Figure 7 Mean connectivity value in (A) the direct connections and (B) other connections for Network 1-8 using connectivity metrics CC, ACC-i, PC and PCC

Therefore, to examine the impact of the indirect connections on each connectivity method in greater detail, we separately quantified the average connectivity values in the direct connections compared to all other connections in each iteration (Figure 7). Direct connections are node pairs with $\varepsilon_{ij} = 0.5$, and all other connections are $\varepsilon_{ij} = 0$. Here, we exclude the results from ACC-e because its values are all close to zero. PC shows the best distinction between direct connections (high connectivity values) and indirect connections (low connectivity values) in most networks. The mean direct connectivity values of ACC-i were significantly smaller than CC in all cases ($p < 0.05$). The values of PCC were similar to those of PC and ACC-i, which was also true for the Kuramoto model.

For the non-direct connections (including both indirect and unconnected nodes), the mean connectivity values are surprisingly consistent in the four metrics, fluctuating around 0.05 (Figure 7B). This could be related to the 95% threshold in the significance testing. The threshold values for significant connections are chosen as the 95% threshold in a null distribution, where the alternate hypothesis is that there is a temporal relationship between the signals from the two electrodes. Therefore, there is a 5% chance of false positive in the significance testing, and this approximately matches the 0.05 connectivity values for the indirect or uncoupled connections. Therefore, these low values indicate that each connectivity method is correctly determining these nodes to be uncoupled.

6.3 Human EEG data

6.3.1 Comparison between connectivity method

We compared functional connectivity head maps for each connectivity metric and age group in the same brain state. Generally, the frontal and occipital connections were stronger than

connections in the other brain regions during sleep stage N2 (or QS for Group A) (Figure 8). This feature was evident for all connectivity measurements, except for ACC-e in Group A. Missing connections in the occipital lobe in Group A could be caused by the overall weaker connectivity values in that group compared to the other age groups. When we applied group-specific thresholds, the same pattern of strong frontal and occipital connections emerged in group A as well. Similar results during wakefulness are shown in the Appendix B.

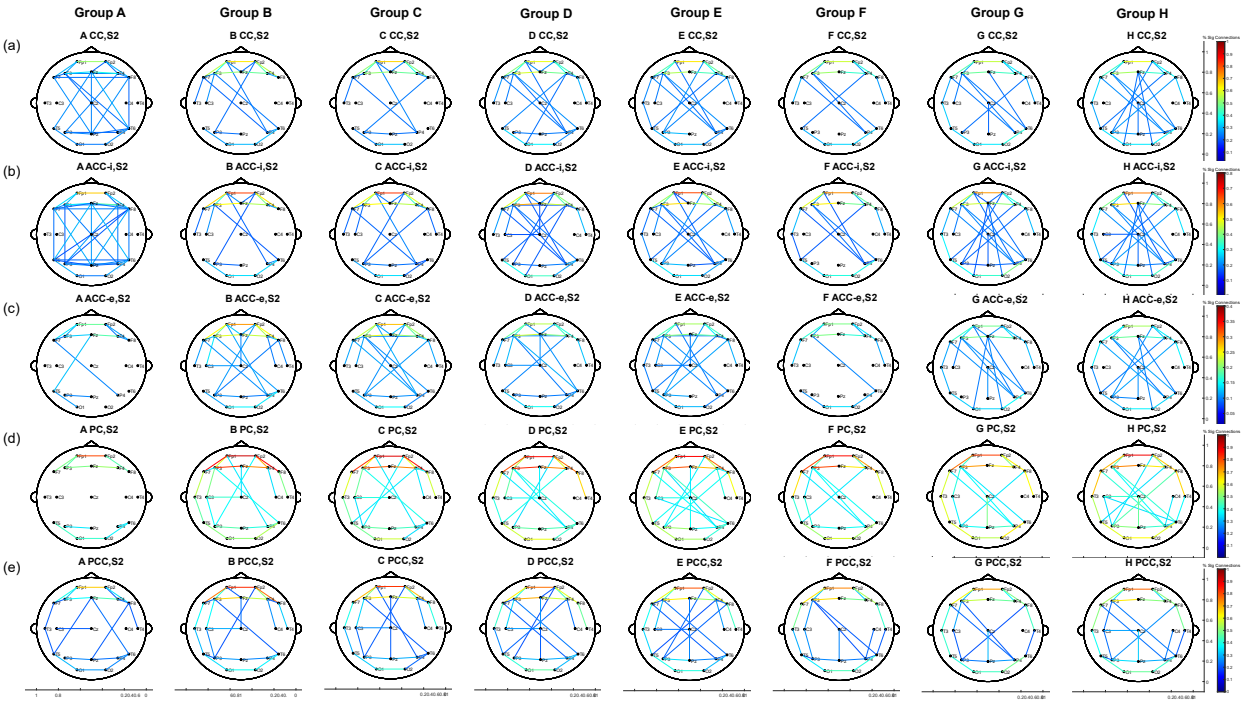

Figure 8 Functional Connectivity Networks in sleep stage N2, constructed by (a) CC, (b) ACC-i, (c) ACC-e, (d) PC, and (e) PCC. The column from left to right corresponds to group A to H.

FCNs measured by CC and ACC-i are similar (Figure 8 (a), (b)), and both metrics show insufficiency in identifying true connections. For example, both metrics show intrahemispheric connections between the frontal and temporal lobes in Group A. Those connections are not present for any of the multivariate metrics nor ACC-e. Also, it is expected that infants at 0-3 months have overall lower connectivity values, as is shown in the results of multivariate

measurements and ACC-e. Those evidence suggests that FCNs constructed by CC and ACC-i produce spurious connections, possibly caused by volume conduction. Another example is that CC and ACC-i recognize all connections between F4, T5, and O1 as significant in Group D, whereas the other three metrics only recognize connections between F4-T5 and T5-O1 (Figure 8). It indicates that the correlation between O1 and F4 could be driven by the confounding variable T5; note that the multivariate metrics and ACC-e successfully eliminate the effect from it and recover the actual connection. These results show the need for methods such as ACC-e or multivariate measurements to avoid misleading results.

The effect of including and excluding values at zero lag can be seen by comparing Figure 8(b) and 8(c). First, the amplitude of the average connectivity decreases by 50% when excluding values at zero lag. It is consistent with the results in the simulation study that ACC-e systematically underestimates the connectivity values in the system. Also, the edge densities (i.e., the ratio between the number of existing edges and all possible edges) in Group B and C are higher for ACC-e than ACC-i, while those in other groups are lower for ACC-e than ACC-i. The decrease in edge density from ACC-i to ACC-e is expected, and it holds for all other groups. Groups B and C may exhibit the opposite trend because the abnormal intrahemispheric connections between the frontal and temporal lobes in Group A increases the overall threshold in ACC-i. As groups B and C have lower average connectivity values, more connections are excluded for those two groups, causing an overall decrease in the edge density.

FCNs measured by PC have higher connectivity values compared to all other metrics. The head maps are characterized by strong short-range connections between the outermost electrodes. The connectivity values of PC are very high, especially for connection between Fp1 and Fp2. The value is close to or equal to one, meaning that all epochs of all the subjects in an

age group measure the connection to be significant. This is similar to the results for the Rössler model, in which PC had the highest distinction between true connections and background noise.

Chapter 7 Discussion

Using both simulated and human EEG data, we compared the functional connectivity networks calculated by bivariate and multivariate metrics, including a new method based on partial cross-correlation. The results from the Rössler model and human EEG share several key features. In both cases, multivariate metrics have larger connectivity values compared to bivariate metrics. This can be explained by the simulation results in the Rössler model. What we find in the Rössler model is that the average connectivity values in the direct connections are higher for multivariate metrics than the bivariate metrics, while the mean values of indirect and uncoupled connections are similar in all measurements. This is likely because the null distribution of connection strength based on surrogate data used for significance testing also accounts for the effect of volume conduction in bivariate metrics. Systems with a stronger influence from volume conduction will also have higher threshold values (Shahbazi Forooz and Ewald, 2010).

The simulation results from the Kuramoto model contradict the Rössler model and human EEG data in several ways. For example, the multivariate metrics and ACC-e underestimate the true coupling strengths in the system, whereas the results from cross-correlation and ACC-I coincide with the actual degree of synchrony. This may be because the oscillators in the Kuramoto model were all weakly coupled, while the Rössler model and real EEG data contained stronger connections (Hale et al., 2012; Lainscsek et al., 2013). Multivariate measures consider the correlation between two variables while eliminating the confounding effect from other similar variables. Hence, if oscillators are globally coupled, the multivariate correlation will decrease when accounting for the similarity in other variables. Although the results from the Kuramoto model differ from the real EEG data, the results from the Kuramoto model provide

valuable information, especially when comparing the adjusted cross-correlation including and excluding values at zero lag. The performance of ACC-e is more comparable to that of the multivariate metrics than the other bivariate metrics. It indicates that the adjusted cross-correlation produces a valid connectivity network when zero lag connections are excluded, and significance testing is applied to each epoch (Chu et al., 2012). In a real EEG system, coupling strength affected by volume conduction has a synchronous phase relationship, while true coupling could happen at zero phase lag as well (Vinck et al., 2011). Hence, we expect that ACC-e has a higher false-negative rate in detecting significant connections and is even more stringent than multivariate metrics.

Limitations of the study can be addressed in the future. First, linear mixing of the signal is a naïve method to model volume conduction because it only considers relationships at zero phase lag in the signal propagation. However, volume conduction involves a more complex situation related to the isotropic conductivities and the shape of the brain (Huiskamp et al., 1999). Thus, applying a forward model to the simulated data while considering all these factors may provide more insight than the linear mixing method (Vermaas et al., 2020). Moreover, the signal-to-noise ratio was reported to affect the results of connectivity measurements (Silfverhuth et al., 2012), but we have not included this as a parameter in our simulations. Consequently, the simulation parameters should be considered carefully in order to most closely resemble the human EEG signals.

In this thesis, we compare functional connectivity networks constructed from bivariate and multivariate metrics. We also propose a new metric, the partial cross-correlation. The results show that PC, PCC, and ACC-e are all valid choices for EEG systems. ACC-e is the most computationally efficient one, but it has the highest false-negative rate. For PC, we have

implemented the first-order calculation, and it has been shown to provide the best performance against volume conduction in both simulated and human EEG. A possible improvement is to implement a higher-order PC that yields more precise results but also increases the computation time (Liu et al., 2016). PCC is the most time-consuming method, 1000 times slower than ACC and 100 times slower than PC. The distribution of connection strength shares similar properties with cross-correlation, while the functional connectivity networks are comparable to those of partial correlation. Overall, no distinct advantages of PCC were found over the other metrics.

Reference

Agastinose Ronicko, J. F., Thomas, J., Thangavel, P., Koneru, V., Langs, G., & Dauwels, J. (2020). Diagnostic classification of autism using resting-state fMRI data improves with full correlation functional brain connectivity compared to partial correlation. *Journal of Neuroscience Methods*, *345*.

https://doi.org/10.1016/j.jneumeth.2020.108884

Ahmadi, N., Pei, Y., & Pechenizkiy, M. (2019). Effect of linear mixing in EEG on synchronization and complex network measures studied using the Kuramoto model. *Physica A: Statistical Mechanics and Its Applications*, *520*, 289–308. https://doi.org/10.1016/j.physa.2019.01.003

Al-Khassaweneh, M., Villafane-Delgado, M., Mutlu, A. Y., & Aviyente, S. (2016). A Measure of Multivariate Phase Synchrony Using Hyperdimensional Geometry. *IEEE Transactions on Signal Processing*, *64*(11), 2774–2787.

https://doi.org/10.1109/TSP.2016.2529586

Babaeeghazvini, P., Rueda-Delgado, L. M., Gooijers, J., Swinnen, S. P., & Daffertshofer, A. (2021). Brain Structural and Functional Connectivity: A Review of Combined Works of Diffusion Magnetic Resonance Imaging and Electro-Encephalography. *Frontiers in Human Neuroscience*, *15*.

https://doi.org/10.3389/fnhum.2021.721206

Bastos, A. M., & Schoffelen, J.-M. (2016). A Tutorial Review of Functional Connectivity Analysis Methods and Their Interpretational Pitfalls. *Frontiers in Systems Neuroscience*, *9*, 175.

https://doi.org/10.3389/fnsys.2015.00175

Borbely, A. A., Baumann, F., Brandeis, D., Strauch, I., & Lehmann, D. (1981). Sleep Deprivation: Effect on Sleep Stages and EEG Power Density in Man. *Electroencephalography and Clinical Neurophysiology*, *51*(5), 483–493. https://doi.org/https://doi.org/10.1016/0013-4694(81)90225-X.

Briels, C. T., Briels, C. T., Schoonhoven, D. N., Schoonhoven, D. N., Stam, C. J., de Waal, H., Scheltens, P., & Gouw, A. A. (2020). Reproducibility of EEG functional connectivity in Alzheimer's disease. *Alzheimer's Research and Therapy*, *12*(1). https://doi.org/10.1186/s13195-020-00632-3

Brunner, C., Billinger, M., Seeber, M., Mullen, T. R., Makeig, S., Lansky, P., Cohen, M. X., & Özkurt, T. E. (2016). Volume conduction influences scalp-based connectivity estimates. *Frontiers in Computational Neuroscience*, *10*(NOV). https://doi.org/10.3389/fncom.2016.00121

Chu, C. J., Kramer, M. A., Pathmanathan, J., Bianchi, M. T., Westover, M. B., Wizon, L., & Cash, S. S. (2012). Emergence of stable functional networks in long-term human electroencephalography. *Journal of Neuroscience*, *32*(8), 2703–2713. https://doi.org/10.1523/JNEUROSCI.5669-11.2012

Cohen, M. X. (2014). Power-Based Connectivity. In *Analyzing Neural Time Series Data: Theory and Practice* (pp. 357–370). MIT Press. https://doi.org/https://doi.org/10.7551/mitpress/9609.003.0034

Cumin, D., & Unsworth, C. P. (2007). Generalising the Kuramoto model for the study of neuronal synchronisation in the brain. *Physica D: Nonlinear Phenomena*, *226*(2), 181–196. https://doi.org/10.1016/j.physd.2006.12.004

Durka, P. J., Klekowicz, H., Blinowska, K. J., Szelenberger, W., & Niemcewicz, S. (2003). A simple system for detection of EEG artifacts in polysomnographic recordings. *IEEE Transactions on Biomedical Engineering*, *50*(4), 526–528. https://doi.org/10.1109/TBME.2003.809476

Fitzgibbon, S. P., Pope, K. J., MacKenzie, L., Clark, C. R., & Willoughby, J. O. (2004). Cognitive tasks augment gamma EEG power. *Clinical Neurophysiology*, *115*(8), 1802–1809. https://doi.org/10.1016/j.clinph.2004.03.009

Hale, A. C., Hansard, T., Sheppard, L. W., McClintock, P. V. E., & Stefanovska, A. (2012). The Kuramoto model subject to a fluctuating environment: Application to brainwave dynamics. *Fluctuation and Noise Letters*, *11*(1). https://doi.org/10.1142/S0219477512400111

Haufe, S., Nikulin, V. v., Müller, K. R., & Nolte, G. (2013). A critical assessment of connectivity measures for EEG data: A simulation study. *NeuroImage*, *64*(1), 120–133. https://doi.org/10.1016/j.neuroimage.2012.09.036

Huiskamp, G., Vroeijenstijn, M., van Dijk, R., Wieneke, G., & van Huffelen, A. C. (1999). The need for correct realistic geometry in the inverse EEG problem. *IEEE Transactions on Biomedical Engineering*, *46*(11), 1281–1287. https://doi.org/10.1109/10.797987

Hyde, J. S., & Jesmanowicz, A. (2012). Cross-correlation: An fMRI signal-processing strategy. In *NeuroImage* (Vol. 62, Issue 2, pp. 848–851). https://doi.org/10.1016/j.neuroimage.2011.10.064

Ibáñez-Molina, A. J., & Iglesias-Parro, S. (2016). Neurocomputational model of EEG complexity during mind wandering. *Frontiers in Computational Neuroscience*, *10*(MAR). https://doi.org/10.3389/fncom.2016.00020

Imperatori, C., Farina, B., Adenzato, M., Valenti, E. M., Murgia, C., Marca, G. della, Brunetti, R., Fontana, E., & Ardito, R. B. (2019). Default mode network alterations in individuals with high-trait-anxiety: An EEG functional connectivity study. *Journal of Affective Disorders*, *246*, 611–618. https://doi.org/10.1016/j.jad.2018.12.071

Jalili, M., & Knyazeva, M. G. (2011a). Constructing brain functional networks from EEG: Partial and unpartial correlations. *Journal of Integrative Neuroscience*, *10*(2), 213–232. https://doi.org/10.1142/S0219635211002725

Jalili, M., & Knyazeva, M. G. (2011b). EEG-based functional networks in schizophrenia. *Computers in Biology and Medicine*, *41*(12), 1178–1186. https://doi.org/10.1016/j.compbiomed.2011.05.004

Jameson, L. C., & Sloan, T. B. (2006). Using EEG to monitor anesthesia drug effects during surgery. In *Journal of Clinical Monitoring and Computing* (Vol. 20, Issue 6, pp. 445–472). https://doi.org/10.1007/s10877-006-9044-x

Kiiski, H., Rueda-Delgado, L. M., Bennett, M., Knight, R., Rai, L., Roddy, D., Grogan, K., Bramham, J., Kelly, C., & Whelan, R. (2020). Functional EEG connectivity is a neuromarker for adult attention deficit hyperactivity disorder symptoms. *Clinical Neurophysiology*, *131*(1), 330–342.

https://doi.org/10.1016/j.clinph.2019.08.010

Kramer, M. A., Eden, U. T., Cash, S. S., & Kolaczyk, E. D. (2009). Network inference with confidence from multivariate time series. *Physical Review E - Statistical, Nonlinear, and Soft Matter Physics*, *79*(6).

https://doi.org/10.1103/PhysRevE.79.061916

Kumagai, Y., Arvaneh, M., Okawa, H., Wada, T., & Tanaka, T. (2017). Classification of familiarity based on cross-correlation features between EEG and music. *Proceedings of the Annual International Conference of the IEEE Engineering in Medicine and Biology Society, EMBS*, 2879–2882.

https://doi.org/10.1109/EMBC.2017.8037458

Kuramoto, Y. (1984). *Chemical Oscillations, Waves, and Turbulence*. Springer-Verlag.

Lainscsek, C., Weyhenmeyer, J., Hernandez, M., Poizner, H., & Sejnowski, T. (2013). Non-Linear Dynamical Classification of Short Time Series of the Rössler System in High Noise Regimes. *Frontiers in Neurology*, *4*, 182.

https://doi.org/10.3389/fneur.2013.00182

Liu, Y., Zhao, Q., Chen, M., & Zhang, L. (2016). Higher-order correlation coefficient analysis for EEG-based brain-computer interface. *Frontiers in Artificial Intelligence and Applications*, *285*, 1080–1088.

https://doi.org/10.3233/978-1-61499-672-9-1080

Lu, C. M., Zhang, Y. J., Biswal, B. B., Zang, Y. F., Peng, D. L., & Zhu, C. Z. (2010). Use of fNIRS to assess resting state functional connectivity. *Journal of Neuroscience Methods*, *186*(2), 242–249.

https://doi.org/10.1016/j.jneumeth.2009.11.010

Michelini, G., Jurgiel, J., Bakolis, I., Cheung, C. H. M., Asherson, P., Loo, S. K., Kuntsi, J., & Mohammad-Rezazadeh, I. (2019). Atypical functional connectivity in adolescents and adults with persistent and remitted ADHD during a cognitive control task. *Translational Psychiatry*, *9*(1).

https://doi.org/10.1038/s41398-019-0469-7

Moretti, D. v, Babiloni, F., Carducci, F., Cincotti, F., Remondini, E., Rossini, P. M., Salinari, S., Babiloni, C., & Risoluzione, A. (2003). Computerized processing of EEG-EOG-EMG artifacts for multi-centric studies in EEG oscillations and event-related potentials. *International Journal of Psychophysiology*, *47*(3), 199–216. https://doi.org/https://doi.org/10.1016/s0167-8760(02)00153-8.

Nguyen, P. T. M., Hayashi, Y., Baptista, M. D. S., & Kondo, T. (2020). Collective almost synchronization-based model to extract and predict features of EEG signals. *Scientific Reports*, *10*(1).

https://doi.org/10.1038/s41598-020-73346-z

Nunez, P. L., Srinivasan, R., & Fields, R. D. (2015). EEG functional connectivity, axon delays and white matter disease. *Clinical Neurophysiology*, *126*(1), 110–120. https://doi.org/10.1016/j.clinph.2014.04.003

Omidvarnia, A., Azemi, G., Boashash, B., Otoole, J. M., Colditz, P. B., & Vanhatalo, S. (2014). Measuring time-varying information flow in scalp EEG signals: Orthogonalized partial directed coherence. *IEEE Transactions on Biomedical Engineering*, *61*(3), 680–693. https://doi.org/10.1109/TBME.2013.2286394

Paula, A., de Oliveira, S., Araújo De Santana, M., Karoline, M., Andrade, S., Gomes, J. C., Rodrigues, M. C. A., & dos Santos, W. P. (2020). Early diagnosis of Parkinson's disease using EEG, machine learning and partial directed coherence. *Research on Biomedical Engineering*.

https://doi.org/10.1007/s42600-020-00072-w/Published

Peraza, L. R., Asghar, A. U. R., Green, G., & Halliday, D. M. (2012). Volume conduction effects in brain network inference from electroencephalographic recordings using phase lag index. *Journal of Neuroscience Methods*, *207*(2), 189–199. https://doi.org/10.1016/j.jneumeth.2012.04.007

Righi, G., Tierney, A. L., Tager-Flusberg, H., & Nelson, C. A. (2014). Functional connectivity in the first year of life in infants at risk for autism spectrum disorder: An EEG study. *PLoS ONE*, *9*(8).

https://doi.org/10.1371/journal.pone.0105176

Ruiz-Gómez, S. J., Gómez, C., Maturana-Candelas, A., Rodríguez-González, V., García, M., Tola-Arribas, M. A., Cano, M., & Hornero, R. (2019). Analysis of Volume Conduction Effects on Different Functional Connectivity Metrics: Application to Alzheimer's Disease EEG Signals. *2019 41st Annual International Conference of the IEEE Engineering in Medicine and Biology Society (EMBC)*.

https://doi.org/10.0/Linux-x86_64

Ruiz-Gómez, S. J., Hornero, R., Poza, J., Maturana-Candelas, A., Pinto, N., & Gómez, C. (2019). Computational modeling of the effects of EEG volume conduction on functional connectivity metrics. Application to Alzheimer's disease continuum. *Journal of Neural Engineering*, *16*(6).

https://doi.org/10.1088/1741-2552/ab4024

Ryali, S., Chen, T., Supekar, K., & Menon, V. (2012). Estimation of functional connectivity in fMRI data using stability selection-based sparse partial correlation with elastic net penalty. *NeuroImage*, *59*(4), 3852–3861.

https://doi.org/10.1016/j.neuroimage.2011.11.054

Sakkalis, V. (2011). Review of advanced techniques for the estimation of brain connectivity measured with EEG/MEG. *Computers in Biology and Medicine*, *41*(12), 1110–1117. https://doi.org/10.1016/j.compbiomed.2011.06.020

Schmidt, H., Petkov, G., Richardson, M. P., & Terry, J. R. (2014). Dynamics on Networks: The Role of Local Dynamics and Global Networks on the Emergence of Hypersynchronous Neural Activity. *PLoS Computational Biology*, *10*(11). https://doi.org/10.1371/journal.pcbi.1003947

Shahbazi Forooz and Ewald, A. and Z. A. and N. G. (2010). Constructing Surrogate Data to Control for Artifacts of Volume Conduction for Functional Connectivity Measures. In A. Supek Selma and Sušac (Ed.), *17th International Conference on Biomagnetism Advances in Biomagnetism – Biomag2010* (pp. 207–210). Springer Berlin Heidelberg. https://doi.org/10.1007/978-3-642-12197-5_46

Shahsavari Baboukani, P., Azemi, G., Boashash, B., Colditz, P., & Omidvarnia, A. (2019). A novel multivariate phase synchrony measure: Application to multichannel newborn EEG analysis. *Digital Signal Processing: A Review Journal*, *84*, 59–68. https://doi.org/10.1016/j.dsp.2018.08.019

Silfverhuth, M. J., Hintsala, H., Kortelainen, J., & Seppänen, T. (2012). Experimental comparison of connectivity measures with simulated EEG signals. *Medical and Biological Engineering and Computing*, *50*(7), 683–688. https://doi.org/10.1007/s11517-012-0911-y

Smith, R. J., Alipourjeddi, E., Garner, C., Maser, A. L., Shrey, D. W., & Lopour, B. A. (2021). Infant functional networks are modulated by state of consciousness and circadian rhythm. *Network Neuroscience*, 1–17.

https://doi.org/10.1162/netn_a_00194

Smith, S. J. M. (2005). EEG in the diagnosis, classification, and management of patients with epilepsy. In *Neurology in Practice* (Vol. 76, Issue 2).

https://doi.org/10.1136/jnnp.2005.069245

Stam, C. J., Nolte, G., & Daffertshofer, A. (2007). Phase lag index: Assessment of functional connectivity from multi channel EEG and MEG with diminished bias from common sources. *Human Brain Mapping*, *28*(11), 1178–1193.

https://doi.org/10.1002/hbm.20346

Sun, F. T., Miller, L. M., & D'Esposito, M. (2004). Measuring interregional functional connectivity using coherence and partial coherence analyses of fMRI data. *NeuroImage*, *21*(2), 647–658.

https://doi.org/10.1016/j.neuroimage.2003.09.056

Sunwoo, J. S., Lee, S., Kim, J. H., Lim, J. A., Kim, T. J., Byun, J. I., Jeong, M. H., Cha, K. S., Choi, J. W., Kim, K. H., Lee, S. T., Jung, K. H., Park, K. il, Chu, K., Kim, M., Lee, S. K., & Jung, K. Y. (2017). Altered functional connectivity in idiopathic rapid eye movement sleep behavior disorder: A resting-state EEG study. *Sleep*, *40*(6).

https://doi.org/10.1093/sleep/zsx058

Vakulin, A., D'Rozario, A., Kim, J. W., Watson, B., Cross, N., Wang, D., Coeytaux, A., Bartlett, D., Wong, K., & Grunstein, R. (2016). Quantitative sleep EEG and polysomnographic predictors of driving simulator performance in obstructive sleep apnea. *Clinical Neurophysiology*, *127*(2), 1428–1435.

https://doi.org/10.1016/j.clinph.2015.09.004

Vermaas, M., Piastra, M. C., Oostendorp, T. F., Ramsey, N. F., & Tiesinga, P. H. E. (2020). FEMfuns: A Volume Conduction Modeling Pipeline that Includes Resistive, Capacitive or Dispersive Tissue and Electrodes. *Neuroinformatics*, *18*(4), 569–580. https://doi.org/10.1007/s12021-020-09458-8

Vinck, M., Oostenveld, R., van Wingerden, M., Battaglia, F., & Pennartz, C. M. A. (2011). An improved index of phase-synchronization for electrophysiological data in the presence of volume-conduction, noise and sample-size bias. *NeuroImage*, *55*(4), 1548–1565. https://doi.org/10.1016/J.NEUROIMAGE.2011.01.055

Wang, J., Ethridge, L. E., Mosconi, M. W., White, S. P., Binder, D. K., Pedapati, E. v., Erickson, C. A., Byerly, M. J., & Sweeney, J. A. (2017). A resting EEG study of neocortical hyperexcitability and altered functional connectivity in fragile X syndrome Refining translational treatment development in fragile X syndrome. *Journal of Neurodevelopmental Disorders*, *9*(1).

https://doi.org/10.1186/s11689-017-9191-z

Zhang, Y., Wu, W., Toll, R. T., Naparstek, S., Maron-Katz, A., Watts, M., Gordon, J., Jeong, J., Astolfi, L., Shpigel, E., Longwell, P., Sarhadi, K., El-Said, D., Li, Y., Cooper, C., Chin-Fatt, C., Arns, M., Goodkind, M. S., Trivedi, M. H., … Etkin, A. (2021). Identification of

psychiatric disorder subtypes from functional connectivity patterns in resting-state electroencephalography. *Nature Biomedical Engineering*, *5*(4), 309–323. https://doi.org/10.1038/s41551-020-00614-8

Appendix A The ratio of connections that happen at zero lag.

Network	% of connections happen at zero lag	% of above threshold connections have zero lag
1	12.1	65.0
2	21.9	80.9
3	31.3	90.6
4	41.3	99.4
5	40.2	98.6
6	46.5	99.4
7	62.6	99.96
8	84.3	100

Appendix B Functional Connectivity Networks during wakefulness